Wave-front Sensing and correction for 4-meter LAMOST

Xi Zhang*[a, b, c], Deqing Ren[a, b, d], Yongtian Zhu[a, b], Jiangpei Dou[a, b, c]
[a]National Astronomical Observatories/Nanjing Institute of Astronomical Optics & Technology, Chinese Academy of Science, Nanjing 210042, China;
[b]Key Laboratory of Astronomical Optics & Technology, National Astronomical Observatories/Nanjing Institute of Astronomical Optics & Technology, Chinese Academy of Science, Nanjing 210042, China;
[c]Graduate School of the Chinese Academy of Sciences, Beijing 100049, China;
[d]Physics & Astronomy Department, California State University Northridge, 18111 Nordhoff Street, Northridge, California 91330

ABSTRACT

LAMOST is a 4m spectroscopic telescope recently operational at Xinglong, China. Several active optics are being used to remove optical aberration of the telescope, but large residual aberration exists since the active optics actuators on the telescope's segmented mirrors cannot provide enough precision. We proposed a wave-front sensing system and the corresponding algorithm to measure this low frequency residual aberration. We developed a compact Shack-Hartmann wave-front sensor that can use point source as well as extended structure images for wave-front sensing and can achieve good measurement accuracy. The wave-front sensing algorithm is realized by LabVIEW that is based on block-diagram programming and is suitable for rapid prototype development. Combined with deformable mirrors, the system will be able to provide a fine wave-front correction and therefore eventually remove the residual aberration for LAMOST. The wave-front sensor and the DMs will also be used for our high-contrast imaging coronagraph to remove speckle noise for the direct imaging of exoplanets.

Keywords: wave-front sensing, residual aberration, LAMOST, LabVIEW

1. INTRODUCTION

LAMOST is a 4m spectroscopic telescope recently operational at Xinglong Station, Beijing. The optics system of LAMOST consists of a spherical primary mirror Mb at the southern end, a reflecting Schmidt corrector Ma at the northern end and the focal plane as well [1], shown in Fig.1. Mb and Ma are composed of 37 and 24 hexagonal sub-mirrors respectively. A thin deformable mirror active optics on Ma is used to form the 24 sub-mirrors into required aspherical surface shape to eliminate the 3rd order spherical aberration of the primary mirror Mb. Two segmented mirror active optics on Mb and Ma are used to control the 24 sub-mirrors and the 37 sub-mirrors to keep co-focus respectively [2].

Astronomical and Space Optical Systems, edited by Penny G. Warren, Cheryl J. Marshall, Robert K. Tyson, Michael Lloyd-Hart, James B. Heaney, E. Todd Kvamme, Proc. of SPIE Vol. 7439, 74390V · © 2009 SPIE · CCC code: 0277-786X/09/$18 · doi: 10.1117/12.825417

Downloaded from SPIE Digital Library on 22 Jan 2010 to 159.226.100.232. Terms of Use: http://spiedl.org/terms

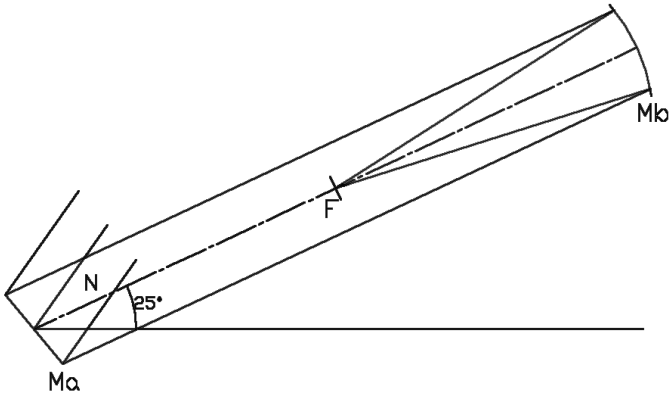

Fig.1. The layout of the optical system of LAMOST

The current active optics actuators can not provide enough precision to eliminate all the wave-front errors of LAMOST system and large residual aberration exists. For direct imaging of Exoplanets by using LAMOST in future, we proposed a wave-front sensing system and a corresponding algorithm to measure this residual aberration. We also discussed the correction of residual piston aberration of the segmented primary mirror Mb.

2. Wave-front sensing and correction

2.1 Compact Shack-Hartmann Wave-front Sensor

We developed a compact Shack-Hartmann wave-front sensor (S-H WFS) for the associated measurements. The compact S-H WFS is composed of a square micro-lenses array with the size of 10mm×10mm, radius of curvature of 8.6mm and lens pitch of 300μm, an USB CCD video camera, shown in Fig.2 and Fig.3. Incident wave-fronts are focused by every micro lenses onto the CCD chip to form a sub-images array. The micro-lenses array is fixed in a black anodized aluminum tube (shown in Fig.3) that can be adjusted to change the distance between the micro-lenses array and the CCD chip.

Downloaded from SPIE Digital Library on 22 Jan 2010 to 159.226.100.232. Terms of Use: http://spiedl.org/terms

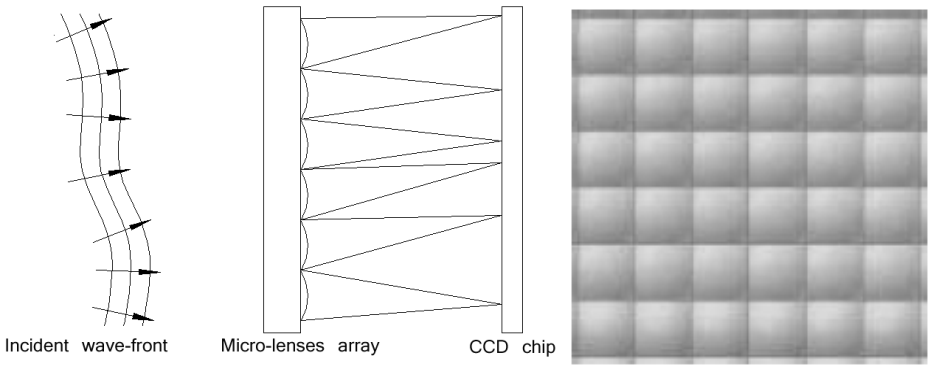

Fig.2. The compact S-H WFS. Left: the configuration of the sensor. Right: the micro-lenses array.

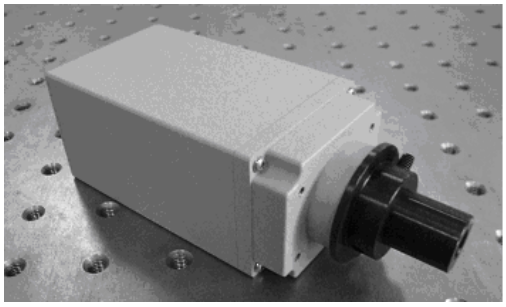

Fig.3. The prototype of the compact S-H WFS

For our laboratorial experiment, we use a laser light with the wavelength of 589.3nm as a point source to perform wave-front calibration and sensing. The WFS should be calibrated with a plane wave-front before a wave-front sensing test. The experimental optical layout is shown in Fig.4: the expanded laser beam is collimated and compressed by a series of 3 lenses to fit the size of the circle aperture of the micro-lenses array and forms an incident plane wave-front. Such an optical layout can be combined with other optical paths by adding a beam splitter between the Lens a and Lens b. An optical layout that will be used for our later experiments is shown in Fig.5: the optical layout shown in Fig.4 will be fixed to do calibration and the wave-front errors will be offered by the DM. The whole system is also available for sensing and correcting the static aberration of the DM. The S-H WFS we developed can also use extended structure images for wave-front sensing, thus it is possible to use this S-H WFS to do solar wave-front sensing of which the object source could be sunspots.

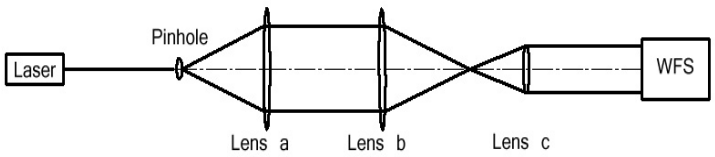

Fig.4. The experimental optical layout

Downloaded from SPIE Digital Library on 22 Jan 2010 to 159.226.100.232. Terms of Use: http://spiedl.org/terms

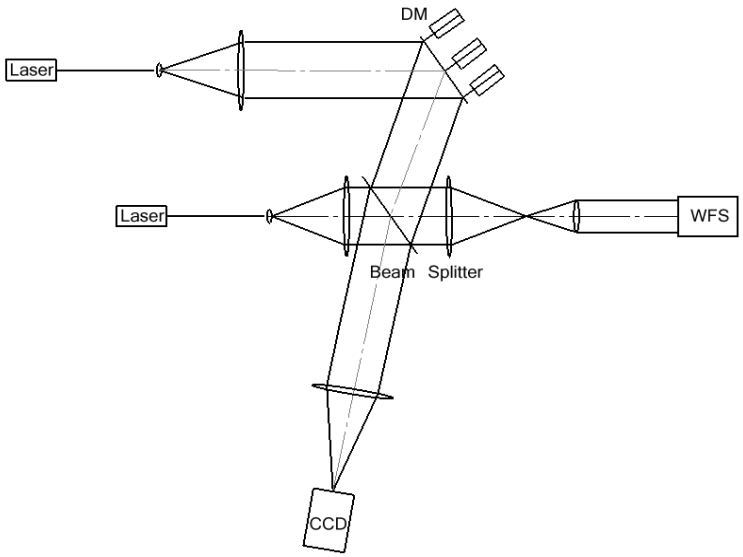

Fig.5. The experimental optical layout with DM

2.2 Wave-front sensing algorithm

The wave-front to be detected can be described by Zernike polynomials,

$$\phi = \sum_{k=1}^{K} a_k Z_k(x,y) \tag{1}$$

where $Z_k(x, y)$ is the k th mode of Zernike function and the Zernike coefficients a_k stand for the magnitude of the corresponding wave-front errors. The first 6 normalized Zernike functions used in our algorithm are shown in Table.1.

Table.1 The first 6 Zernike functions

Mode	Zernike function	Meaning
1	1	Piston
2	y	tip
3	x	tilt
4	2xy	astigmatism
5	$2(x^2+y^2)-1$	defocus
6	x^2-y^2	astigmatism

The slopes of a wave-front in two orthogonal directions can be described by the following equations [3],

Downloaded from SPIE Digital Library on 22 Jan 2010 to 159.226.100.232. Terms of Use: http://spiedl.org/terms

$$\frac{\partial \phi}{\partial x} = \sum_{k=1}^{K} a_k \frac{\partial Z_k(x,y)}{\partial x}$$
$$\frac{\partial \phi}{\partial y} = \sum_{k=1}^{K} a_k \frac{\partial Z_k(x,y)}{\partial y} \tag{2}$$

For m total measurements at various positions, the slope vector **s** and Zernike coefficient vector **a** have the relationship of **s=[B]a**, where

$$s = \begin{pmatrix} \left.\frac{\partial \phi}{\partial x}\right|_1 \\ \left.\frac{\partial \phi}{\partial x}\right|_2 \\ \vdots \\ \left.\frac{\partial \phi}{\partial x}\right|_m \\ \left.\frac{\partial \phi}{\partial y}\right|_1 \\ \left.\frac{\partial \phi}{\partial y}\right|_2 \\ \vdots \\ \left.\frac{\partial \phi}{\partial y}\right|_m \end{pmatrix}, a = \begin{pmatrix} a_1 \\ a_2 \\ a_3 \\ \vdots \\ a_k \end{pmatrix} \tag{3}$$

and the matrix **[B]** is

$$[B] = \begin{pmatrix} \left.\frac{\partial Z(x,y)_1}{\partial x}\right|_1 & \left.\frac{\partial Z(x,y)_2}{\partial x}\right|_1 & \cdots & \left.\frac{\partial Z(x,y)_K}{\partial x}\right|_1 \\ \left.\frac{\partial Z(x,y)_1}{\partial x}\right|_2 & \left.\frac{\partial Z(x,y)_2}{\partial x}\right|_2 & \cdots & \left.\frac{\partial Z(x,y)_K}{\partial x}\right|_2 \\ \vdots & \vdots & & \vdots \\ \left.\frac{\partial Z(x,y)_1}{\partial x}\right|_m & \left.\frac{\partial Z(x,y)_2}{\partial x}\right|_m & \cdots & \left.\frac{\partial Z(x,y)_K}{\partial x}\right|_m \\ \left.\frac{\partial Z(x,y)_1}{\partial y}\right|_1 & \left.\frac{\partial Z(x,y)_2}{\partial y}\right|_1 & \cdots & \left.\frac{\partial Z(x,y)_K}{\partial y}\right|_1 \\ \vdots & \vdots & & \vdots \\ \left.\frac{\partial Z(x,y)_1}{\partial y}\right|_m & \left.\frac{\partial Z(x,y)_2}{\partial y}\right|_m & \cdots & \left.\frac{\partial Z(x,y)_K}{\partial y}\right|_m \end{pmatrix} \tag{4}$$

The vector **s** can be acquired by subtracting the corresponding coordinates between the measurement image and the reference image,

Downloaded from SPIE Digital Library on 22 Jan 2010 to 159.226.100.232. Terms of Use: http://spiedl.org/terms

$$S = \begin{pmatrix} \Delta x_1 \\ \Delta x_2 \\ \vdots \\ \Delta x_m \\ \Delta y_1 \\ \Delta y_2 \\ \vdots \\ \Delta y_m \end{pmatrix}, \Delta x_i = x_i' - x_i, \quad \Delta y_i = y_i' - y_i, (i = 1,2,\cdots,m) \tag{5}$$

where (x_i', y_i') and (x_i, y_i) stand for the normalized coordinates of the i th sub-images in the two images respectively. To calculate $\mathbf{a} = [\mathbf{B}]^{-1}\mathbf{s}$, and the pseudo-inverse of **[B]** is given by

$$[B]^{-1} = VS^{-1}U^T \tag{6}$$

where U, S and V are the singular value decomposition of [B] which is $[B]=USV^T$ [1].

In our experiment, a total number of 97 square sub-apertures (97 positions for measuring wave-front slopes) are used to fit a real circle aperture shown in Fig.6, and we will expand the sub-aperture number in our later work. 66 modes of Zernike polynomials are used to describe an incident wave-front: it is precise enough for most cases of wave-front sensing and the number of modes can be chosen freely in the program.

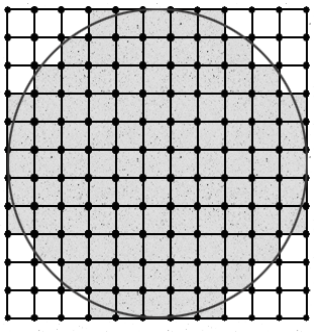

Fig.6. Illustration of the sub-apertures: the gray squares stand for sub-apertures, the black spots stand for actuators if a DM is added, the big circle is the real aperture.

The wave-front sensing algorithm was realized by using LabVIEW software that offers various function modules and is based on block-diagram programming. Prototype developments based on this software is fast and convenient: costs of the developments can be reduced and the precision and speed of calculation that is important to our code can be ensured. By using the "pattern match" module offered by LabVIEW, the center coordinates of each sub-image from a sub-images array can be acquired and the wave-front slopes of every sub-aperture can be calculated. The flow chart of our wave-front sensing code is shown in Fig.7.

Downloaded from SPIE Digital Library on 22 Jan 2010 to 159.226.100.232. Terms of Use: http://spiedl.org/terms

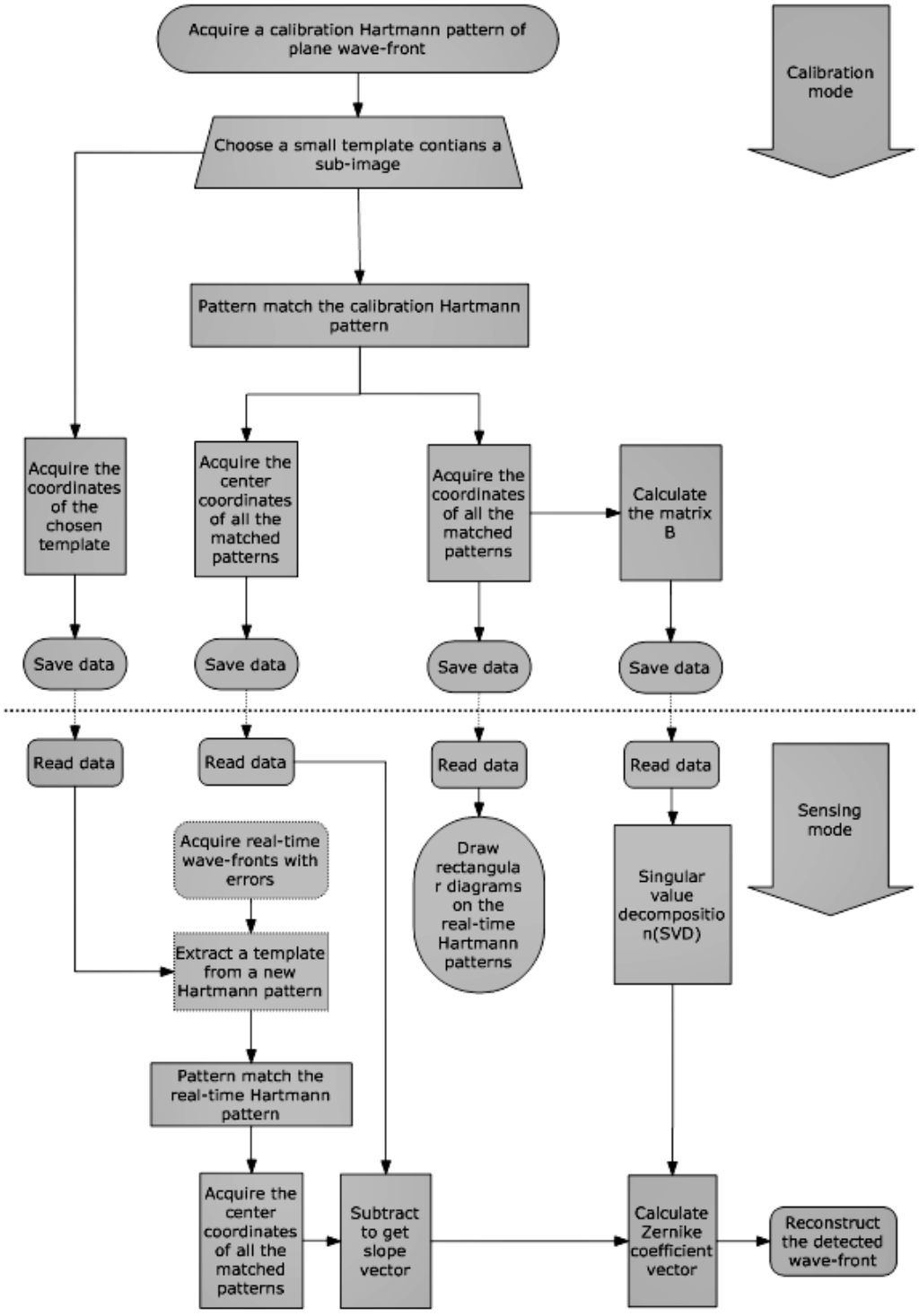

Fig.7. The flow chart of the wave-front sensing code

The code runs under “calibration mode” and “sensing mode”. Only a point source can be used under the “calibration mode”, but both a point source and an extended structure image can be used under the “sensing mode”. For the “calibration mode”, the optical path should be precisely adjusted to lead a

Downloaded from SPIE Digital Library on 22 Jan 2010 to 159.226.100.232. Terms of Use: http://spiedl.org/terms

plane wave-front into the WFS. Based on the calibration sub-images array of the plane wave-front, the code will acquire and save the data including the coordinates of two diagonal points of a square template that is manually chosen, the coordinates of two diagonal points of each sub-aperture pattern matched by the chosen template, the center coordinates of all sub-images, the matrix **[B]** calculated according to the center coordinates of all sub-images. Unless the current optics layout is changed, the later wave-front sensing test can be achieved by directly running the code under the "sensing mode" that will read all the data saved under the "calibration mode" and use them to extract a template from a new sub-images array and do pattern match in real-time scale. The slope vector **s** and Zernike coefficient vector **a** will be calculated under the "sensing mode" and a wave-front will be reconstructed based on the vector **a**. Meanwhile, a sub-aperture array represented by rectangular diagrams is drawn in the real-time scale according to the data of the calibration sub-aperture pattern saved before. The front panel of the code (Fig.8.) shows a series of Zernike coefficients a_k , a sub-images array with the sub-aperture array and the reconstructed wave-front.

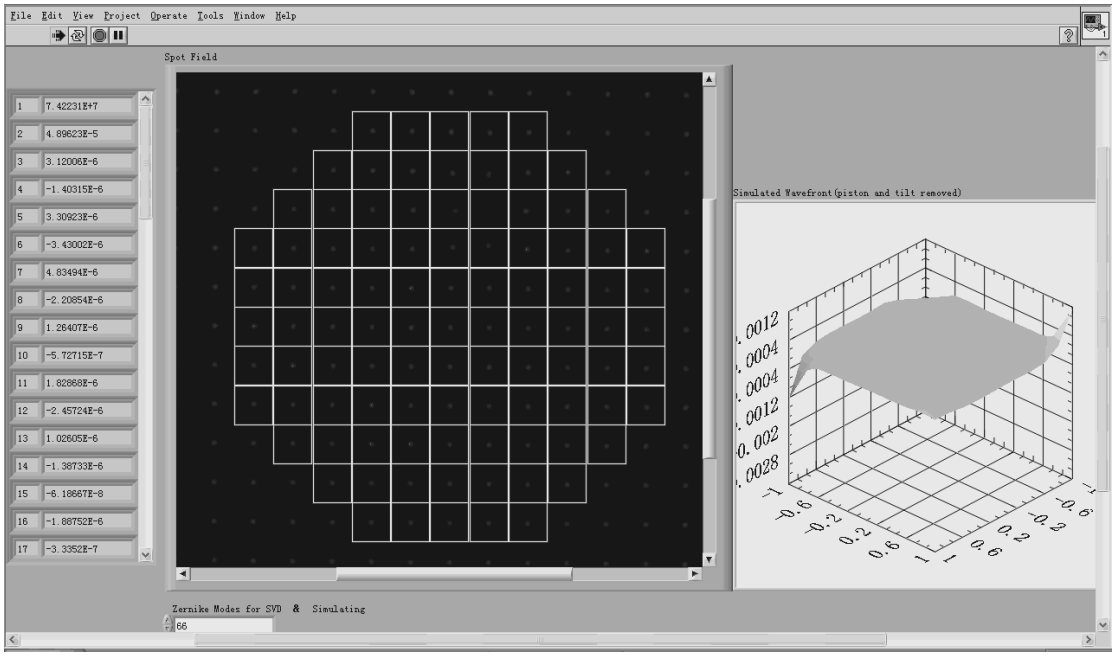

Fig.8. The front panel of the code: a sensing test for plane wave-fronts is running.

2.3 Wave-front sensing and correction of piston and tip-tilt aberrations

According to the scientific goals of LAMOST, only co-focus is needed for all the sub-mirrors of Ma and Mb [4] and has been achieved by two independent segment mirror active optics of which the S-H WFS are respectively installed at the focus of LAMOST and at the curvature center of Mb and three displacement actuators with 6mm working travel and 50nm motion resolution are installed at the back of each sub-mirror [4-5]. For future imaging observation and adding focal plane instruments such as coronagraphs for direct imaging exoplanets, the co-phase of Ma and Mb is necessary. LAMOST can

Downloaded from SPIE Digital Library on 22 Jan 2010 to 159.226.100.232. Terms of Use: http://spiedl.org/terms

apply the technique of narrowband and broadband Shack-Hartmann phasing [6] that has been implemented on the Keck telescopes. However, a special diffractive-lenses array that fits the alignment of the segmented mirrors (shown in Fig. 10) should be designed and the directly corrections on the telescope's primary mirror still leave large residual aberration.

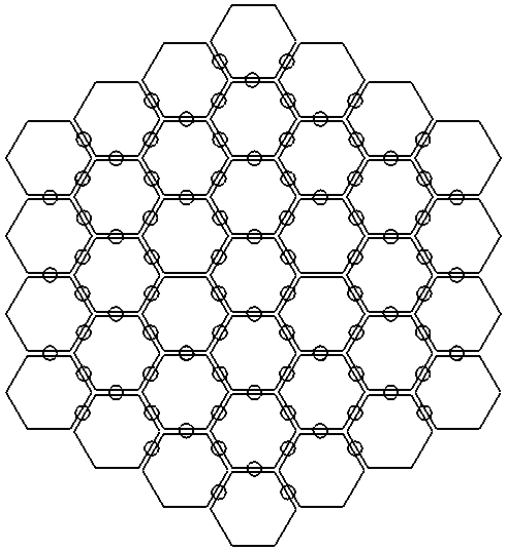

Fig.10. The diffractive-lenses array for sensing piston errors applied on the Keck telescopes [7]: LAMOST can adopt the similar design.

We proposed another co-phase method to measure and correct the piston and tip-tilts errors of segmented mirrors. The miss-alignment of a segment mirror with piston error and tip-tilts error leads to an incident wave-front with defocus component and tip-tilts component detected by the WFS: the defocus component takes a large proportion comparing to the tip-tilts component for the piston error case and vice versa for the tip-tilts error case. Fig.11 illustrates the relationships of the incident defocused wave-front, the piston error and the tip-tilts error of a segment mirror respectively. The two kinds of errors can be measured by analyzing the defocus component and tip-tilts component that are represented as Zernike coefficients. For the 37 sub-mirrors of Mb with different magnitudes of piston and tip-tilts errors, a sub-images array of the whole primary mirror can be acquired by the compact WFS and divided into 37 areas corresponding to the sub-mirrors respectively; the wave-front sensing algorithm will run in the each area to calculate the Zernike coefficients of defocus and tip-tilts that evaluate the piston error and the tip-tilts error of the sub-mirror.

Downloaded from SPIE Digital Library on 22 Jan 2010 to 159.226.100.232. Terms of Use: http://spiedl.org/terms

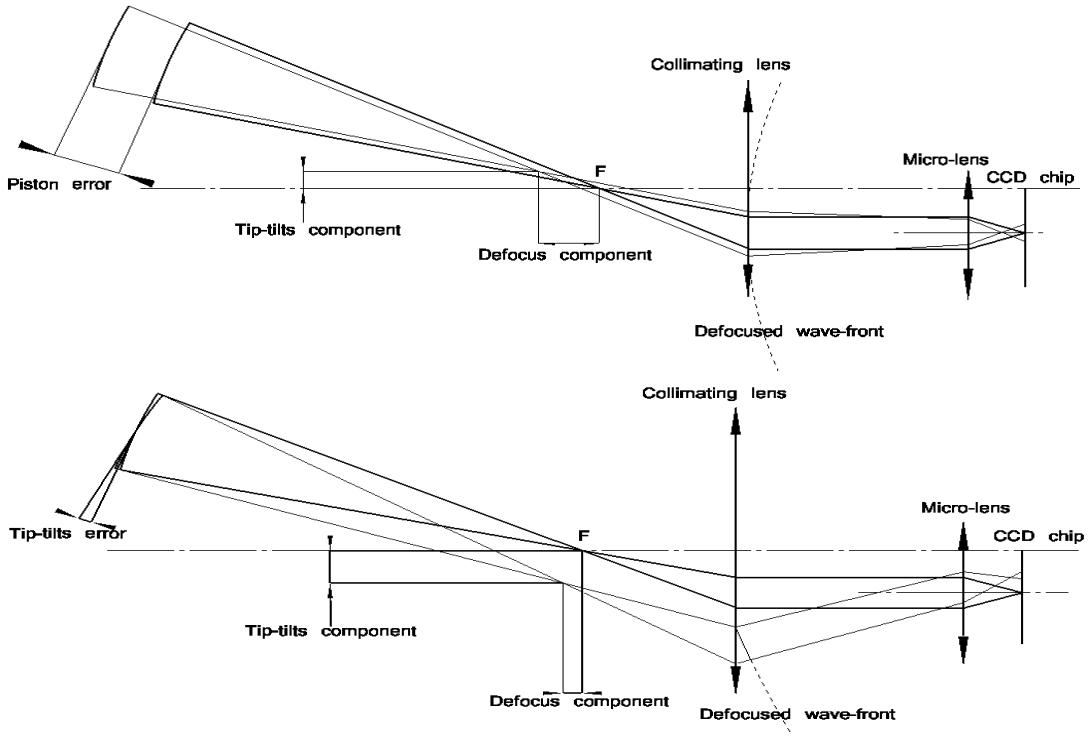

Fig.11. Up: piston error of a segment mirror leads to a defocused wave-front with small tip-tilts component. Down: tip-tilts error of a segment mirror leads to a tip-tilted wave-front with small defocus component.

The piston difference and the tip-tilts differences between two adjacent sub-mirrors with serial number of i and j are approximately described as,

$$\Delta tip^{i\to j} = k_y(c_y^i a_2^i - c_y^j a_2^j) \tag{7}$$

$$\Delta tilt^{i\to j} = k_x(c_x^i a_3^i - c_x^j a_3^j) \tag{8}$$

$$\Delta piston^{i\to j} = k_d(c_d^i a_5^i - c_d^j a_5^j) \tag{9}$$

where a_2, a_3 and a_5 are the Zernike coefficients according to the Table.1; k_x, k_y, k_d are the scaling factors that relate to the wave-front sensing system; c_x, c_y, c_d are the incline factors that relate to the sub-mirrors. In fact, the measured differences of piston and tip-tilts are contributed by both of the defocus component and the tip-tilts component and the effect is more obvious at brinks of the primary mirror, so the sub-mirror located in center of the primary mirror can be selected as a

Downloaded from SPIE Digital Library on 22 Jan 2010 to 159.226.100.232. Terms of Use: http://spiedl.org/terms

"calibration mirror" with the serial number of zero. Considering measurement errors e_x, e_y and e_d, the calibrated piston and tip-tilts errors can be described as,

$$\Delta tip^{i\to 0} = k_y(c_y^i a_2^i - c_y^0 a_2^0) + k_y(e_y^i - e_y^0) \tag{10}$$

$$\Delta tilt^{i\to 0} = k_x(c_x^i a_3^i - c_x^0 a_3^0) + k_x(e_x^i - e_x^0) \tag{11}$$

$$\Delta piston^{i\to 0} = k_d(c_d^i a_5^i - c_d^0 a_5^0) + k_d(e_d^i - e_d^0) \tag{12}$$

since each sub-mirror are analyzed independently, the measurement errors will not accumulate to a high level comparing to the method that directly analyzes the relative piston and tip-tilts between two sub-mirrors. By using this method, 6 modes of Zernike function are enough to analyze the piston and tip-tilts errors and only 3 sampling points are needed for the each sub-mirror.

A segmented DM that is optically conjugated to the primary mirror can be used for correcting the primary mirror, which is composed of a sub-mirrors array with the same arrangement and figuration of the telescope's sub-mirrors. Each of the sub-mirrors is responsible for offering independent piston/tip/tilt motions according to the calibrated errors of its sub-mirror. Since the measured piston and tip-tilts errors are approximations to the real values, one time of wave-front sensing and correction may not give a best compensation. The solution is to alternately correct the measured defocus component and tip-tilts components and form a closed-loop system shown in Fig.12. The similar correction is available for Ma, and two sets of segmented deformable mirrors can be installed to respectively achieve the co-phase of Ma and Mb.

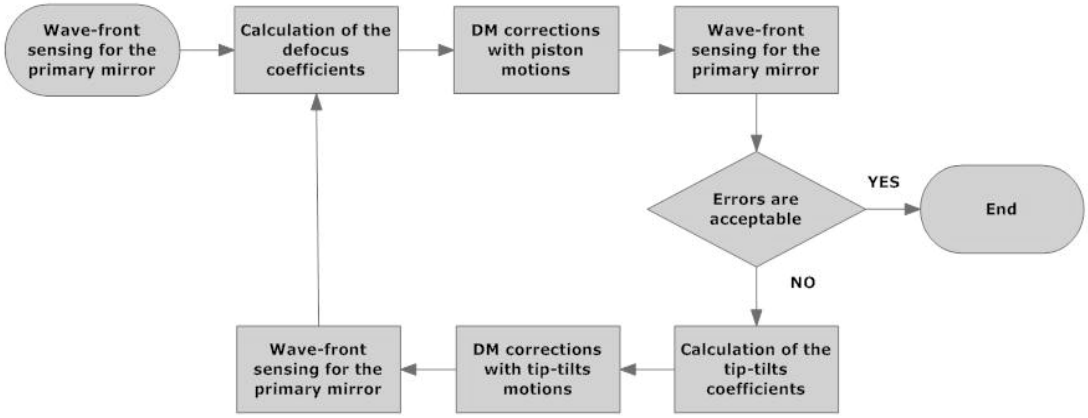

Fig.12. The flow chart of sensing and correcting wave-front errors of LAMOST

For our future plan of using LAMOST for searching exoplanets, the segmented DM can also correct the wave-front errors caused by atmospheric turbulence. The correction is important as the seeing of Xinglong Station is about 2" [1]. And for the coronagraph we are developing, such a DM can help to null the speckle noise and provide an extra gain of contrast. According to the focal plane wave-front

Downloaded from SPIE Digital Library on 22 Jan 2010 to 159.226.100.232. Terms of Use: http://spiedl.org/terms

sensing algorithm for high contrast imaging we proposed, the DM can supply an additional compensative phase based on the wave-front sensing result of coronagraph system to create a dark hole served as a discovery area for planet imaging [7].

3. Conclusions

The wave-front sensing system we proposed is available for measure the aberration of LAMOST. Combined with two segmented deformable mirrors designed for the Ma and Mb mirrors of LAMOST, the piston and tip-tilts errors can be corrected. An algorithm of sensing the telescope's residual aberration by filtering atmospheric turbulence error should be derived. We expect to test this wave-front sensing system and the new algorithm on LAMOST and report our latest progress in the near future.

REFERENCES

[1] Xiangyuan Yan, Xiangqun Cui, Genrong Liu, Yong Zhang, Yongjun Qi, "Low-order AO system in LAMOST," Proc. SPIE 6272, pp. 62723O, (2006).

[2] Xiangqun Cui, "Progress and prospect of LAMOST project," Proc. SPIE 6267, pp. 626703, (2006).

[3] Robert K. Tyson, "Principles of Adaptive Optics," ACADEMIC PRESS, 264-266(1998).

[4] Dingqiang Su, Xiangqun Cui, "Active Optics in LAMOST," Chin.J Astron Astrophys, Vol.4 (1), 1-9(2004).

[5] Dehua Yang, Yongjun Qi, "Measurement of the Actuation Transmitting Mechanism of the Segment Prototype of the LAMOST Telescope," Proc. SPIE 5877, pp. 295-306, (2005).

[6] Gary A. Chanan, Mitchell Troy, Catherine M. Ohara, "Phasing the primary mirror segments of the Keck telescopes: a comparison of different techniques," Proc. SPIE 4003, 188-202, (2000).

[7] Malbet F., Yu J.W, Shao M, "High dynamic range imaging using a deformable mirror for space coronagraph", PASP, 107, pp. 386 (1995).

Downloaded from SPIE Digital Library on 22 Jan 2010 to 159.226.100.232. Terms of Use: http://spiedl.org/terms